Novel Calcium Phosphate Glass for Hard-Tissue Regeneration

Yong-Keun Lee[1*], Seong-Ho Choi[2]

1. Department and Research Institute of Dental Biomaterials and Bioengineering, Yonsei University College of Dentistry

2. Department of Periodontology, Research Institute for Periodontal Regeneration, Yonsei University College of Dentistry

ABSTRACT

Purpose: The aim of this review is to introduce a novel bone-graft material for hard-tissue regeneration based on the calcium phosphate glass(CPG).

Materials and Methods: CPG was synthesized by melting and subsequent quenching process in the system of $CaO-CaF_2-P_2O_5-MgO-ZnO$ having a much lower Ca/P ratio than that of conventional calcium phosphates such as HA or TCP. The biodegradability and bioactivity were performed. Effects on the proliferation, calcification and mineralization of osteoblast-like cells were examined *in vitro*. Influence in new bone and cementum formations was investigated *in vivo* using calvarial defects of Sprague-Dawley rats as well as 1-wall intrabony defect of beagle dogs. The application to the tissue-engineered macroporous scaffold and *in vitro* and *in vivo* tests was explored.

Results: The extent of dissolution decreased with increasing Ca/P ratio. Exposure to either simulated body fluid or fetal bovine serum caused precipitation on the surface. The calcification and mineralization of osteoblast-like cells were enhanced by CPG. CPG promoted new bone and cementum formation in the calvarial defect of Sprague-Dawley rats after 8 weeks. The macroporous scaffolds can be fabricated with 500~800μm of pore size and a three-dimensionally interconnected open pore system. The stem cells were seeded continuously proliferated in CPG scaffold. Extracellular matrix and the osteocalcin were observed at the 2^{nd} days and 4^{th} week. A significant difference in new bone and cementum formations was observed in vivo ($p<0.05$).

Conclusion: The novel calcium phosphate glass may play an integral role as potential biomaterial for regeneration of new bone and cementum. ***(J Korean Acad Periodontol 2008;38:273-298)***

KEY WORDS: calcium phosphate; bone-graft; biodegradable.

Introduction

Phosphate glasses with low dispersion and relatively high refractive indices were developed as achromatic optical elements about 100 years ago by Schott. Subsequent interest stemmed from their high transparency for ultraviolet light. However, the poor chemical durability limited their application and discouraged their further development. In the 1950s, interest in phosphate glass was stimulated by their use in a variety of industrial applications, including sequestering agents for hard water treatments and dispersants for clay processing and pigment manufacturing. The advent of solid state lasers in the 1960s heralded a new era of phosphate glass research. More recently, phosphate glasses have been developed for a variety of specialty applications such as hermetic seals, nuclear waste hosts or solid state electrolytes[1)].

Another important use of phosphate glasses is the application as biomaterials based on the calcium phosphate system. The capacity of the human body to regenerate bone components that are lost, damaged or diseased is limited in several situations. Thus synthetic materials to fill bone defects have been developed. Calcium phosphate materials have some outstanding properties, namely similarity in composition to bane mineral and ostoconductivity. Products in the bone

Correspondence: Yong-Keun Lee, Ph.D.
Department and Research Institute of Dental Biomaterials and Bioengineering, Yonsei University College of Dentistry, 250 Seongsanno, Seodaemun-gu, Seoul 120-752, Korea.
e-mail: leeyk@yuhs.ac, Tel: 82-2-2228-3083, Fax: 82-2-364-9961
* This work was supported by Medical Science and Engineering Research Center (No. R13-2003-13) from the Ministry of Education, Science & Technology.
Received: Jun 27, 2008; Accepted: Aug 1, 2008

graft market based on HA and TCP have been used clinically. However, the success of these materials is limited mainly due to low toughness, low elasticity, low ability to be resorbable and lack of osteogenic properties[2].

Calcium phosphate glass may offer potential for hard tissue surgery because of their solubility behavior, since their solubility may be controlled by altering their chemical composition[3-4]. Its similarities in composition to bone and teeth make them ideal candidates. The good bioactivity and compatibility of the phosphate glasses as potential medical materials attracted the attention of scientists in the field of biomedical research in recent years. An idea of application of calcium phosphate glass-ceramics to the dental crown was proposed firstly by Hosono et al. Calcium phosphate glass-ceramics are interesting biomaterials for bone and tooth implants because of their excellent mechanical strength and castability. Since calcium phosphate glass is easily fused and since the melt has a low viscosity, it is considered to be suitable for casting[5].

The properties that make phosphate glasses candidate for so many different applications are related to their molecular-level structure[1-2]. The basic building blocks of crystalline and amorphous phosphates are the P-tetrahedra that result from the formation of sp^3 hybrid orbitals by the P outer electrons ($3s^2$ $3p^3$). The fifth electron is promoted to a 3d orbital where strong π-bonding molecular orbitals are formed with oxygen 2p electrons. These tetrahedra link through covalent bridging oxygens to form various phosphate anions. The tetrahedral structures are classified using the Q^i terminology, where i represents the number of bridging oxygens per tetradegron. The networks of phosphate glasses can be classified by the oxygen-to-phosphate ratio, which sets the number of tetrahedral linkages, through bridging oxygens, between neighboring P-tetrahedra. Zachariasen identified vitreous P_2O_5 as one of the prototypical 'random network' glass formers. Indeed, recent diffraction studies of v-P_2O_5 are consistent with the Zachariasen description of an open, distorted network of Q^3 tetrahedral. Phosphate glasses can be made with a range of structures, from a cross-linked network of Q^3 tetrahedra (vitreous P_2O_5) to polymer-like metaphosphate chains of Q^2 tetrahedra to invert glasses based on small pyro-(Q^1) and orthophosphate (Q^0) anions, depending on the [O]/[P] ratio as set by glass composition.

Another important property of the calcium phosphate glasses is its ability to dissolve some elements, oxides or biological molecules that are insoluble or poorly soluble in glasses of other materials and crystalline compounds. Thus the calcium phosphate glass is believed to be one of the best approaches to obtain materials of great interest for bony defects associated with the release of biological therapeutic molecules.

The calcium phosphate glasses offer significant advantages, compared to the commonly used biodegradable polymers. They are entirely amorphous. Their degradation rate is predictable and may easily change by altering the composition of the glass[6].

Synthesis of calcium phosphate glass

1. Dissolution and bioactivity

We synthesized amorphous calcium phosphate glass (CPG) by melting and subsequent quenching process. Batches in the system CaO-CaF_2-P_2O_5-MgO-ZnO were prepared with 6 kinds of Ca/P ratios from 0.2 to 1.2 using $CaCO_3$, CaF_2, H_3PO_4, MgO and ZnO as raw materials. The molar ratio of CaO/CaF_2 was fixed to 9 all the time. Both MgO and ZnO were added at 1% in weight, respectively. Mixed batches were dried at 80°C and melted in a platinum crucible at temperatures ranging from 800 to 1550°C depending on the composition. They were subsequently quenched onto the graphite plate at room temperature after melting[7].

In order to determine the crystallinity and crystalline phases of the as-quenched samples, X-ray diffraction analysis was performed using Philips APD

3720 X-ray diffraction apparatus with a fine focus copper target X-ray tube and double crystal monochrometer. There was no crystalline peak up to Ca/P of 0.6 as shown in Fig. 1. When Ca/P ratio was 0.8, the sample exhibited the $Zn_3(PO_4)_2$ as well as $Ca_2P_2O_7$; the former had disappeared but the latter still remained. $Ca_2P_2O_7$ phase partially transformed to $Ca_4P_2O_7$ with increasing Ca/P ratio to 1.2. Crystallinity obtained from the XRD peak intensity decreased with increasing Ca/P ratio.

As-quenched samples were also examined by IR analysis. Absorption spectra were collected using a Perkin-Elmer 983G quadruple grating spectrophotometer with scanning range from 4000 to 400 cm^{-1} after mixing the samples with KBr powder and pressing at 10000 psi in a vacuum. Absorption spectrum with Ca/P of 0.4 showed broad peaks, which is a typical pattern in amorphous glass materials[8-10] as presented in Fig. 2. There were five peaks including four fundamental vibration peaks for the phosphate structure. The first vibration peak of phosphate is the asymmetric stretching mode (ν_3) observed in the range of 1230~1390cm^{-1}, the second vibration peak of phosphate is the symmetric bending mode (ν_4) observed in the frequency range of 780~940cm^{-1}, the third vibration peak of phosphate is the symmetric stretching (ν_1) observed in the frequency range of 530~780cm^{-1}, and the last vibration peak of phosphate is the harmonics of symmetric bending and asymmetric stretching modes (ν_2) observed in the range of 470~800cm^{-1}. Another peak around 1100 cm^{-1} is due to F-O in phosphate [8] originating from CaF_2 as a precursor. The IR peak which changed from broad to sharp shape with increasing Ca/P ratio indicates increasing crystallinity in accordance with the XRD results shown in Fig. 1.

As-quenched samples were reduced either powder less than 10μm or pellets sized 10×10×1mm using ball milling or low speed saw, respectively. Powders were employed in a dissolution test in buffer solutions and pellets were exposed to the simulated body fluid(SBF) as well as fetal bovine serum(FBS). Dissolution properties were investigated in acidic buffer solutions such as 0.1M tris-aminomethane with pH 3 and 7.3 and 0.1M potassium acetate with pH 6 at 37°C by immersing 25mg of powder into 50ml of each buffer solution. The dissolved quantity of Ca^{2+} ions was measured with Metrohm selective calcium ion electrode and automatically transferred to a computer in every 30 sec while continuously stirring at 500rpm with a Caframo RZR 2000 precision digital stirrer. They were recorded during 2, 1 and 4 hrs when the pH of the buffer solutions was 3, 6 and 7.3, respectively. The extent of dissolved Ca^{2+} ions is shown in Fig. 3. Figs. 3(a) and (b) present the dissolved amounts with pH 3 and 7.3 in 0.1M tris-aminomethane solution, respectively, while that after exposure to 0.1M potassium acetate solution with pH 6 is shown in Fig. 3(c). We observed that the lower extent of dissolution decreased with increasing Ca/P ratio in every measurement, possibly due to the decrease of crystallinity. It has already been reported that the amorphous calcium phosphate formed in the plasma-sprayed coatings on dental and orthopedic implants as well as metal substrates had a significant effect on the properties of the coatings; especially it increased the extent of dissolution[11].

Pellet specimens were kept into both 15 ml of SBF and FBS for one week at 37°C. The surface morphology of the pellets was examined by JEOL 5400 scanning electron microscope(SEM) after a thin layer of gold of a few angstrom was coated in a sputter coater both before and after soaking in SBF. After one week of suspension in SBF or FBS, the change of surface morphology examined by SEM is presented in Fig. 4. There was no crystallite on the surface of pellets prior to exposure to SBF or FBS as shown in Fig. 4(a). Tiny crystallites were formed on the surface of pellets after exposure to SBF as shown in Fig. 4(b), while the agglomerated larger crystals were precipitated after suspension in FBS as exhibited in Fig. 4(c). Both crystals were characterized as hydroxyapatite phase by transmission Laue method using H700 Hitachi TEM.

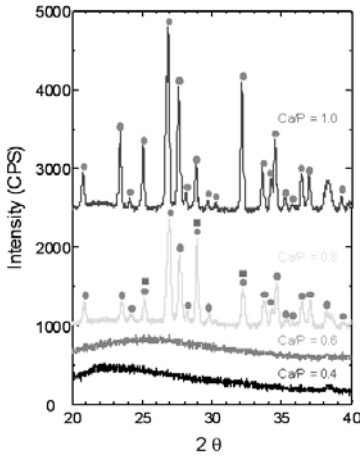

Figure 1. XRD patterns of the as-quenched samples. ● and ■ denote $Ca_2P_2O_7$ and $Zn_3(PO_4)_2$, respectively.

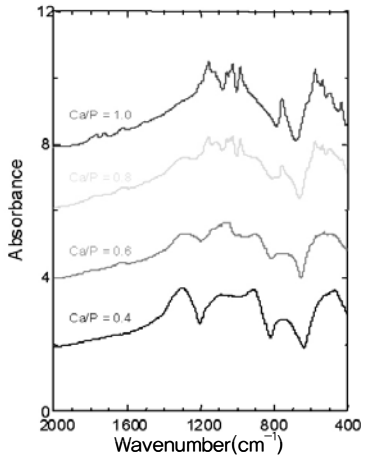

Figure 2. IR absorption spectra of the as-quenched samples.

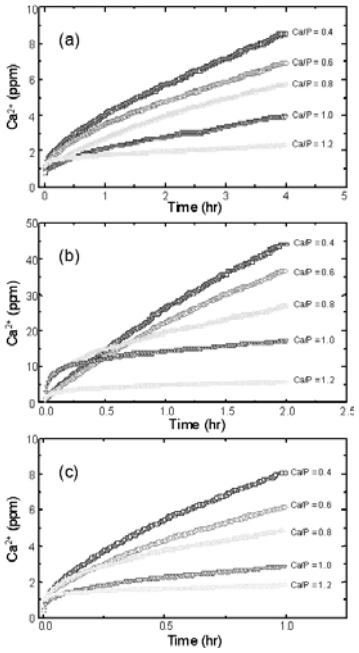

Figure 3. Dissolution of Ca^{2+} ion at 37°C in (a) pH 7.3 and (b) pH 3 in 0.1M tris-aminomethane solution for 2 and 4 hours, respectively, and (c) pH 6 in 0.1M potassium acetate solution for 1 hr.

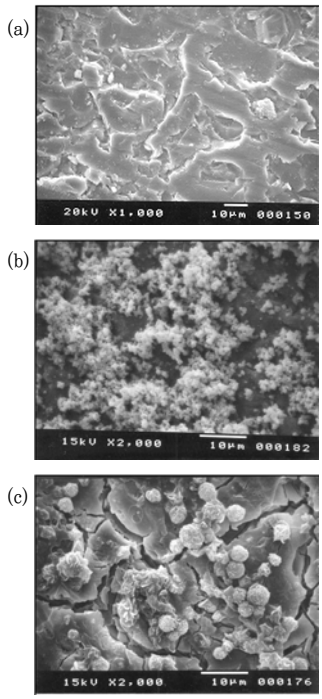

Figure 4. SEM photographs of samples with Ca/P ratio of 0.6 (a) before and after exposure to (b) SBF and (c) FBS for 1 week at 37°C.

2. *In vitro* test

Rectangular pieces of CPG with 10×10×1 mm^3 were employed to in vitro test[12]. Polystyrene in the same dimension was used as control sample. MC3T3-E1 cells extracted from the skull of newborn C57B/6 rats. Sudo *et al*. previously demonstrated that the clonally derived, murine MC3T3-E1 cell line expresses parameters of the osteoblast phenotype, including type I collagen synthesis, alkaline phosphatase and nodular extracellular matrix mineralization resembling woven bone[13]. The cells were maintained in α-modified Eagle's

minimum essential medium (Gibco, NY, USA) supplemented with 10% fetal calf serum (Gibco, NY, USA), 100 U/ml penicillin (Gibco, NY, USA) and 100μg/ml streptomycin (Gibco, NY, USA) in a humidified 5% CO_2 balanced-air incubator at 37°C, the media being changed every other day. In order to induce the spontaneous differentiation into osteoblasts and mineral deposition of MC3T3-E1 cells, 10mMβ-glycerophosphate (Sigma, MO, USA) as well as 50μg/ml ascorbic acid (Sigma, MO, USA) was added to the culture medium since they are known to be essential in osteoblast differentiation in vitro[14].

1) Effect on cell proliferation

MC3T3-E1 cells were seeded into five 6-well tissue culture plates at a density of 1.0×10^5 cells/well in the differentiation medium with calcium phosphate glass or polystyrene and incubated for 2, 4 and 6 days. After each incubation period, the well was dissociated with 0.05 trypsin (Sigma, MO, USA) and 0.5mM EDTA (Sigma, MO, USA), and centrifuged at 1500rpm for 15 min after removal of the culture medium. They were rinsed with Hank's balanced salt solution (HBSS, Sigma, MO, USA) and 400ml of 1% Triton X-100 (Sigma, MO, USA) was added and soaked at 4°C for 30min. The number of cells in each tissue culture plate was directly counted twice with the aid of a hemocytometer under light microscope (CK2, Olympus, Japan). The statistical significant differences of the results between the experimental and control groups were analyzed using an ANOVA with Kruskal-Wallis test at a level of 0.05. The significant differences among the incubation time were analyzed with Mann-Whitney test at a same level.

Changes of number and protein content of MC3T3-E1 cells cultured with and without the prepared non-crystalline calcium phosphate glass are shown in Fig. 5 and Fig. 6, respectively. In all groups, both number and protein content were increased with increasing incubation time ($p<0.05$). They were increased dramatically till the 4th day and the growth rates were somewhat diminished after the 4th day. At every incubation period, there was no significant differences between the experimental and control groups ($p>0.05$). It is suggest that this reduction was not attributed to the toxicity of the prepared calcium phosphate glass, but might be due to the insufficient space of the petri dishes, because the control group also exhibited the same phenomenon, which is well known to be noncytotoxic. Hunter *et al.* reported that the major factor controlling the proliferation rate of the osteoblast cells was the form of cell adhesion, so the reduction of the cell proliferation rate was observed when the cell shape was changed to a spheroid form[15]. In this study, the cell shape was changed to a spheroid form after the mono layer had been formed by the close cell contact, and this result agrees with that of Hunter *et al.*

Owen *et al.* classified the progress of cell differentiation into 3 stages in their study on the differentiation of the osteoblast cells in Sprague-Dawley rats[16]. The initial stage is characterized as cell proliferation and a high level of type I collagen gene expression, biosynthesis, and secretion, but the cells remain undifferentiated as evidenced by low levels of alkaline phosphotase activity, inability to effectively assimilate newly synthesized collagen into extracellular matrix, and the absence of mineralization. Down regulation of the replication and expression of the differentiated osteoblast function is characterized as the second stage, which occurs at approximately the 10th day after plating. The final stage of MC3T3-E1 maturation begins at about the 20th day and is defined by matrix calcification associated with progressive increases in extracellular matrix accumulation and alkaline phosphotase activity. These distinct stages of replication, differentiation, and mineralization in MC3T3-E1 cell cultures are analogous to the respective stages of *in vivo* bone formation, namely, preosteoblast recruitment, osteoblast precursor differentiation to postmitotic matrix-producing osteoblasts, and osteoid mineralization by terminally

differentiated osteoblasts. In this study, based on the dramatic increase of cell proliferation till the 4^{th} day and the slight decrease of the rate at the 6^{th} day, this period is thought to be a transition point from the first stage to the second stage.

2) Effect on alkaline phosphatase activity

In order to evaluate the differentiation of MC3T3-E1 cells quantitatively, alkaline phosphatase(ALP) activity was determined by the method of Lowry[17] every other day during 20 days. 40μL of the centrifuged supernatant was mixed with 2ml of assay kit (No. 245, ALP-10, Sigma, MO, USA), that includes 16mM p-nitrophenyl phosphate. They were seeded in 96-microwell plates at a density of 1.0×10^5 cells/well in the differentiation medium with calcium phosphate glass in 48 wells or polystyrene in the remaining and incubated for 20 days. The optical density at 405nm was measured at both 0.5 and 2.5min after mixing and compared with the value of a series of p-nitrophenol standards. The total cell protein was measured using a commercial assay kit (Bio-Rad, NW, USA) by the method of Bradford[18] and the results expressed in nanomoles of p-nitrophenol produced per min per mg of protein.

The level of alkaline phosphatase activity in the experimental and control groups are shown in Fig. 7. The experimental and control groups exhibited maximum value at the 12^{th} and 8^{th} days, respectively. The activities in the control group at both the 8^{th} and 10^{th} days were significantly higher than at other days ($p<0.05$) and there was no significant differences in the activities among the other days ($p>0.05$). The activities in the experimental group at both the 10^{th} and 12^{th} days were significantly higher than at other days ($p<0.05$). At the same incubation time, the experimental group showed higher activity than in the control group during $10\sim18^{th}$ days ($p<0.05$).

Alkaline phosphotase activity was increased till the 8^{th} day, while it was decreased in the control group. In the experimental group, alkaline phosphotase activity was increased up to the 8^{th} day, similar to the control group, but it was significantly higher than that of the control group during the period from the 10th to 14th days ($p<0.05$). The maximum activity in the experimental group was observed at the 12^{th} day, after which the activity abruptly decreased. Therefore the 8^{th} day is thought to be a transition point from the second stage to the third stage. Gerstenfeld *et al.*[19] and Siffert[20] reported that alkaline phosphatase activity is associated with the maturation of the matrix, but its major role is cell metabolism before bone formation. Another reported role of alkaline phosphatase activity is the formation of bone matrix before the crystallization of the calcium and phosphate ions. The activity is decreased once the calcification starts. The period showing the maximum activity depends on the condition of culture, such as the type of media, and the type and concentration of the enhancing agent for calcification, and the cell concentration in the initial cultivation. According to the reports by El-Ghanuam *et al.*[21] and Itakura *et al.*[22] the activity exhibited the maximum at the 10th day, while it was gradually increased till the 31^{st} day according to Quarles *et al.*[14] Although the results in this study could not be compared directly with those of previous reports, it should be observed that a greater amount of bone nodule was formed in the experimental group than in the control group.

3) Effect on mineralized bone-like tissue formation

After the cell culture which is plated in petri dishes of 100mm diameter reached confluence, i.e. 2.0×10 cells/cm^2, incubated was continued in the differentiation medium for 21 days in a humidified 5% CO_2 balanced-air incubator at 37°C. On day 7, 12, 17 and 21, the cultures in the plates were rinsed using an ice-cooled phosphate buffer saline and fixed with 95% ethyl alcohol. They were stained for 1 hr with 0.1% Alizarin red S (Sigma, MO, USA) to detect the calcium precipitates and followed by subsequent staining with 0.1% light green SF yellowish (Sigma, MO, USA) for

30min to detect the collagen fiber[15]. After rising with 0.1% acetic acid and ethanol, the dual-stained samples were observed under light microscope and the representative pictures were photographed.

Based on the appearance of MC3T3-E1 cells under optical light microscopy, various stages were identified. As shown in Fig. 8, these were composed of growth stage in Fig. 8(a), confluent monolayer stage in Fig. 8(b), and multilayer stage with nodule formation in Fig. 8(c). In order to determine the time of nodule formation, cells were stained with Alizarin red S.

Microscopic examinations were carried out after double-staining with Alizarin red S and light green SF yellow to identify the bone nodule formation. MC3T3-E1 cells grew in a mono layer with a similar shape to the fibroblast cells at the beginning, after which the nodule was formed with multiple layer cells, and finally calcification of the extracellular matrix started. The high alkaline phosphotase activity was investigated in the beginning stage of the nodule formation at the same time. The light green SF yellow is an alkaline staining reagent and is generally used for common cell staining. Alizarin red S is widely used in the study of tissue structure associated with calcium due to its selective calcium binding ability[23]. Since two moles of calcium ions quantitatively bind to a mole of Alizarin red S reagent[24], this staining method is useful in the identification of calcification with a high sensitivity *in vitro*. The center of cells preferring alkaline condition was highly populated in the double-layered cells, so it was stained dark green by light green SF yellow whereas pale green was observed in the outer portion which is located far from the center and has a less dense cell population. As time elapsed the calcification began on the center portion stained with dark green color. Red brown or dark brown were stained at the beginning when calcium was precipitated, and a progressively dark red color was stained for the portion of carrying the great amount of bone nodule. So the center of a cell group stained with green color indicates a starting point of the bone nodule formation where the extracellular matrices are actively formed, and the portion stained with the red color indicates the bone nodule where the calcium was precipitated. Bruijin *et al*. reported that the calcification started from the center portion of the bone nodule, that its size was increased with time, and that it finally gave rise to a different phase between the non-calcified outside of the nodule and the highly calcified inside of the nodule[25]. This portion was called the transition zone which consists of non-fabric particles of 1μm diameter and 250μm thickness. These particles finally aid the adherence of collagen onto the grafted materials, and the transition zone is moved from the center to the outside.

Photographs of MC3T3-E1 cells after staining with Alizarin red S are presented in Fig. 9. Both at the 7th and 12th days, the experimental group showed more abundant green-stained region than in the control group as shown in Figs. 9(a)~(d). At the 17th day, the culture dishes of both the experimental and control groups were almost fully covered with green-stained regions as shown in Figs. 9(e) and 9(f). Small red spots were observed in the experimental group as shown in Fig. 9(f), while there was no red-stained area in the control group. At the 21st day, the control group also exhibited a small red-stained region, as shown in Fig. 9(g). In the experimental group a relatively large, red-stained area was observed especially around the sample, as shown in Fig. 9(h).

Optical photographs are exhibited in Figs. 10 and 11. The nodules could be observed at the 17th and 12th days in the experimental and control groups, respectively. The number of Alizarin red S positive nodules was more abundant in the experimental group at all times in this study.

Microscopic observation after staining was carried out to examine the mineralized bond-like tissue formation. Lots of double-layered bone-like nodules appeared in many portions at the 7th day in the experimental group, while only two portions were observed in the control group. The centered cells had

been changed into the body centered cells of similar size to the osteoblast cells, while the cells located outside of the nodule remained in a similar shape to the fibroblast cells. Since the number of cells and the protein contents were not significantly different between the experimental and control groups ($p>0.05$), it could be concluded that cells were concentrated in the control group but were widely spread in the experimental group. This result might be attributed to the difference of the surface energy between the experimental and control samples. Since the surface energy of the experimental sample was greater than that of the control sample, cells were spread out wide enough to flow down to the petri dish when the cell supernatants had been poured onto the surface of each sample.

The local portion of the mineralized bone-like nodule stained with dark brown color was first observed microscopically at the 12th day in both the experimental and the control groups. The size and number of the nodules were increased with increasing cultivation time, and some of the cells were fused together. A white and opaque membrane visible to the naked eye was formed on the samples at the 17th day. This membrane is considered to be cross-linked collagen fibers originated from the extracellular matrix of the MC3T3-E1 cells[21]. A greater number and quantity of the mineralized bone-like nodules could be observed in the experimental group than in the control group. Alizarin red S positive staining on the sample, observed in the experimental group at the 17th day and in the control group at the 21st day, was widely spread out with time.

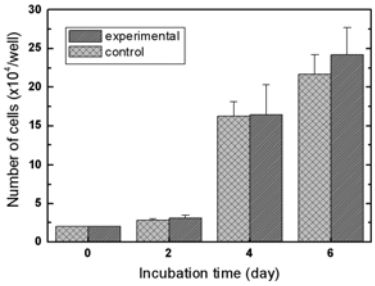

Figure 5. *Number of MC3T3-E1 cells with incubation time.*

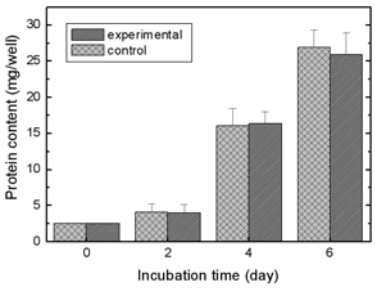

Figure 6. *Protein contents of MC3T3-E1 cells with incubation time.*

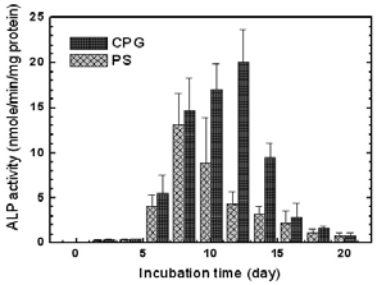

Figure 7. *ALP activities of MC3T3-E1 cells with incubation time.*

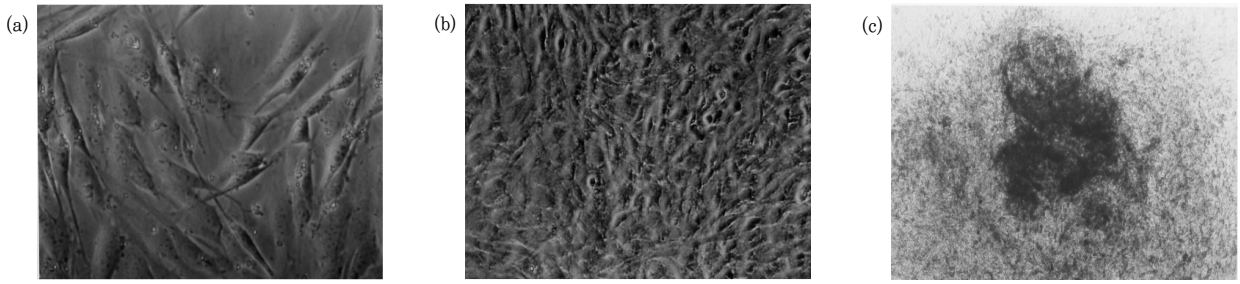

Figure 8. *Micrographs showing the mineralized bone-like tissue formation of MC3T3-E1 cells in the experimental group with incubation time at (a) 2 days(×100), (b) 6 days(×100), and (c) 12 days(×40).*

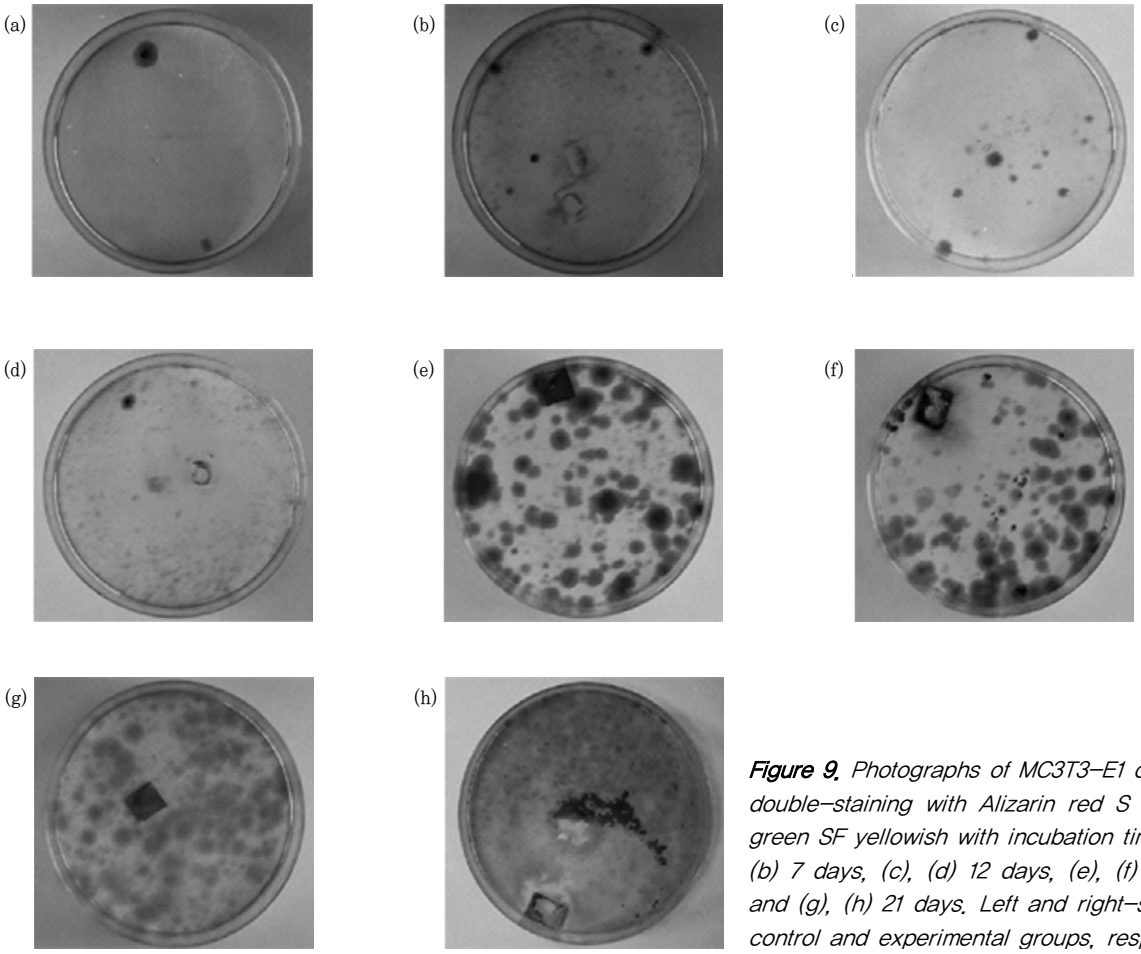

Figure 9. *Photographs of MC3T3-E1 cells after double-staining with Alizarin red S and light green SF yellowish with incubation time of (a), (b) 7 days, (c), (d) 12 days, (e), (f) 17 days, and (g), (h) 21 days. Left and right-sided are control and experimental groups, respectively.*

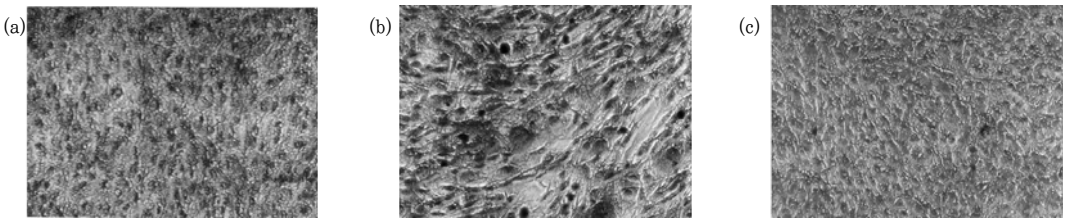

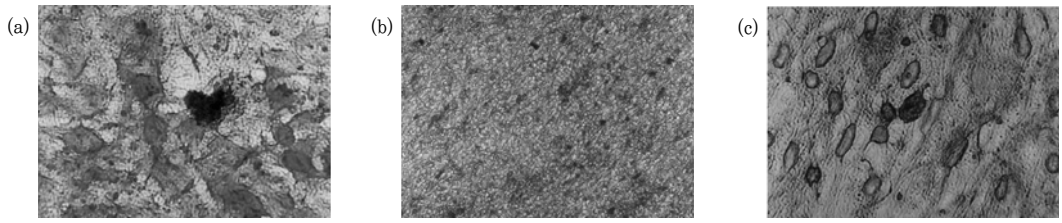

Figure 10. *Histochemical changes of the double-stained MC3T3-E1 cells with Alizarin red S and light green SF yellowish in the control group with incubation time of (a) 7 days(×100), (b) 12 days(×100), (c) 17 days(×100), (d) 17 days(×400), (e) 21 days(×100), and (f) 21 days(×400).*

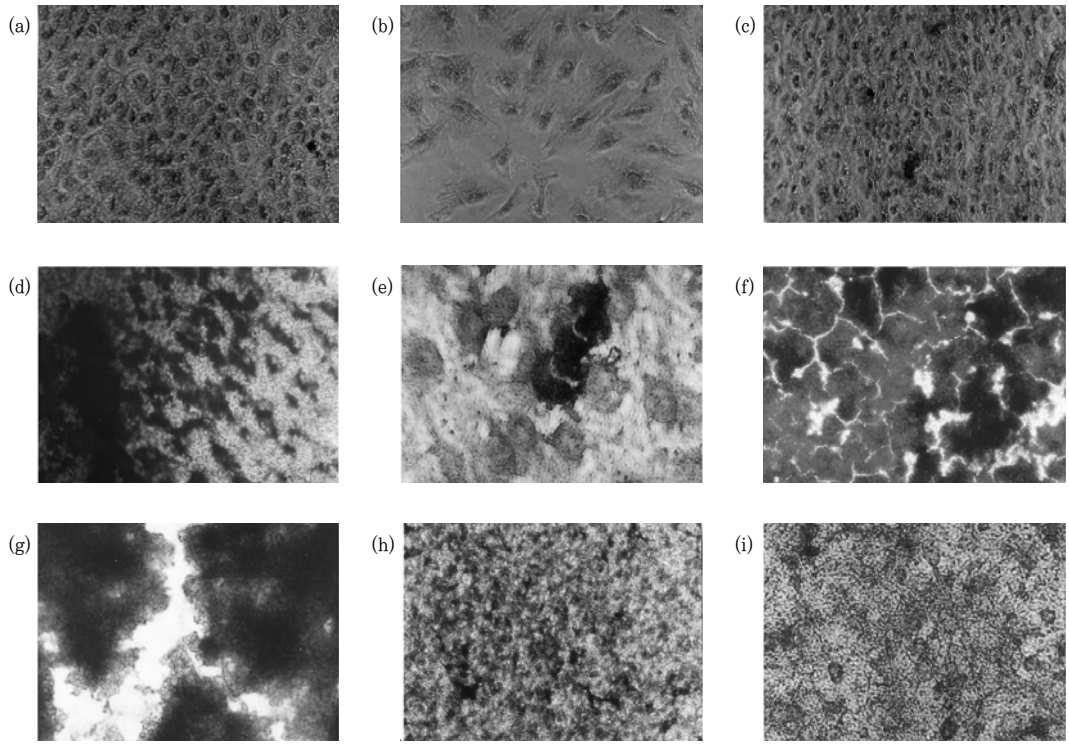

Figure 11. *Histochemical changes of the double-stained MC3T3-E1 cells with Alizarin red S and light green SF yellowish in the experimental group with incubation time of (a) 7 days(×100), (b) 12 days(×100), (c) 17 days(×100), (d) 17 days(×400), (e) 21 days(×100), and (f) 21 days(×400).*

3. *In vivo* test

Sixty male Sprague-Dawley rats (20 per group), weighing 200 to 250g, were used for this experiment. Five animals each were caged with water and food supplied ad libitum. Animal selection and management, surgical protocol, and preparation followed routines approved by the Institutional Animal Care and Use Committee, Yonsei Medical Center, Seoul, Korea[26]. The animals were anesthetized with an intramuscular injection (5mg/kg body weight) consisting of ketamine hydrochloride (Ketalar, Yuhan Co., Seoul, Korea). During surgery, routine infiltration anesthesia was applied at the surgical site using 2% lidocaine (Kwangmyung Pharm., Seoul, Korea) mixed with epinephrine at a ratio of 1:100,000. The surgical site was shaved and scrubbed with iodine. An incision was made in the sagittal plane across the cranium. A

full-thickness flap including the periosteum was reflected, exposing the calvarial bone. Then, a critical-sized (8mm in diameter) circular and transosseous defect, which implies that the defect does not heal by itself during the lifetime of the animal, was created on the cranium using a saline-cooled trephine drill. In addition, we used calvarial defects that had previously been proven to be good models for investigating the effects of bone-graft materials. Freeman and Turnbull were the first to attempt the study of critical-sized defects in rat calvaria[27]. Tagaki and Urist reported that 8mm calvarial defects in six-month-old Sprague-Dawley rats were reduced to 5mm after four weeks and no further healing was noted after 12 weeks[28]. The rat calvarial defect, compared with other experimental bone defects, is a convenient model for studying bone regenerative materials because of its lack of fixation requirements[29]. In addition, the Sprague-Dawley rat defects are both reproducible and native and induced healing processes have been well characterized[30]. Also, 8mm trephine calvarial defects in rats have been shown to be critical-sized defects[28-29, 31-32].

Extreme care was used to avoid injury to the dura mater[29]. Each defect was filled with a constant weight of 0.5g CPG powder, having a mean diameter of 40μm, mixed with saline in the experimental group. As a control, the defect was left empty. The incisions were closed with absorbable sutures. 2, 4 or 8 weeks postsurgery, the animals were sacrificed by CO_2 asphyxiation; they were operated-on and the craniums were carefully dissected free of soft tissue. The craniums were immediately placed into vials and fixed in 10% neutral-buffered formalin for 10 days.

1) Radiodensitometric analysis

All samples were radiographed using a dental X-ray unit (Digora, Soredex, Orion Co., Helsinki, Finland) with an exposure time of 0.1 seconds (70kVp, 7mA). The relative bone density of each radiograph was determined using a computer-assisted Image-Pro Plus System (Media Cybernetics, Silver Spring, MD, USA), as shown in Fig. 12 and the relative bone density was calculated as follows.

Relative bone density (%) =
(bone density in bT-bone density in Oa) /
(bone density in Tc-bone density in Oa) × 100

where, Oa=OT/10; low densitometric reference area
Tc=OT/10; high densitometric reference area
bT=OT/2; determined area in this study

The results of radiodensitometric analysis are shown in Fig. 13. At 2 weeks postsurgery, the mean relative density of new bone for the control and experimental group amounted to (15.88±2.38)% and (30.23±0.88)%, respectively. At 4 weeks postsurgery, the corresponding values were (21.77±6.68)% and (33.66±8.22)%. At 8 weeks postsurgery, they were (26.49±6.48)% and (37.31±10.58)%. Both in the control and experimental groups, the relative bone-fill of the new bone-formed increased with increasing graft duration. However, there were no significant differences between the control group and experimental group ($p<0.05$), except at 8 weeks. Only the control group at 8 weeks showed a significant difference compared to that of 4 weeks ($p<0.05$).

2) Histological observation

Following the radiographic procedures, all samples were decalcified in EDTA-HCl for 7 days and embedded in paraffin. 3μm thick coronal sections through the center of the circular defects were stained with hematoxylin and eosin.

After 2, 4 and 8 weeks in the control group, thin connective tissue was abundant at the defect site, as shown in Fig. 14. Also, there was a minimal quantity of new bone formation originating from the defect margins. The defect center was collapsed.

In the experimental group, 2 weeks after surgery, there were dense, fibrous connective tissues at the

defect site, as shown in Fig. 15. A large number of residual calcium phosphate glass particles were present within the fibrous connective tissue at the defect site. More abundant new bone formation was observed than in the control group. Inflammatory cell infiltration was minimal at the defect site. At 8 weeks, the histological observations were similar to the 2-week observations. Residual calcium phosphate glass particles were fewer in number and the quantity of new bone was greater than that observed at 2 weeks.

The experimental group at 2 weeks showed a clear healing condition. Only minimal inflammatory cell infiltration was observed at the defect site. The calcium phosphate glass powder was partially resorbed and new bone was formed with plenty of dense and fibrous connective tissues. At 8 weeks, the calcium phosphate glass was almost completely resorbed and the defect was nearly completely filled with new-formed bone. In a study reported by Kamakura[33], new bone was formed in the upper side of the defects as well as at the defect margin and the dura mater in the larger powder group, while bone formation was restricted within the defect margin and dura mater in the control and smaller groups. These results by Kamakura indicated that the larger calcium phosphate glass powder is biodegradable in vivo and the larger grafted powder might act to increase osteoconductive activity into the free space and among particles to promote bone regeneration.

3) Histomorphometric analysis

After a conventional microscopic examination, length and area of the new bone formation were measured using a computer-assisted Image-Pro Plus System (Media Cybernetics, Silver Spring, MD, USA). Length and area of the new bone formation were expressed in mm and mm^2, respectively. Statistically significant differences in the results between the experimental and control groups were analyzed using an ANOVA with a Kruskal-Wallis test at a level of 0.05. Significant differences during the sacrifice period were analyzed with a Mann-Whitney test at the same level.

The results of histomorphometric analysis are shown in Fig. 16. At 2 weeks postsurgery, mean length of new bone for the control and experimental group amounted to (0.93±0.07)mm and (1.75±0.10)mm, respectively. At 4 weeks postsurgery, the corresponding values were (1.18±0.19)mm and (2.21±0.13)mm. At 8 weeks postsurgery, they were (1.66±0.14)mm and (2.38±0.13)mm. In both control and experimental groups, the length of new bone-formed increased with increasing graft duration. At 2 weeks postsurgery, mean area of new bone for the control and experimental group amounted to (0.28±0.04)mm^2 and (0.96±0.11)mm^2, respectively. At 4 weeks postsurgery, the corresponding values were (0.46±0.04)mm^2 and (1.41±0.19)mm^2. At 8 weeks postsurgery, they were (0.86±0.09)mm^2 and (1.53±0.18)mm^2. Similar to the length of new bone, in both the control and experimental groups, the area of new bone increased with increasing graft duration. Significant differences between the control group and the experimental group as well as between grafting periods are denoted in Fig. 4. In both the length and area of new bone-formed in all grafting periods, there are significant differences between the control group and experimental group ($p<0.05$). Both control and experimental groups at 4 weeks show significant differences between either 2 weeks and 8 weeks ($p<0.05$), except in the experimental group, it was between 4 weeks and 8 weeks.

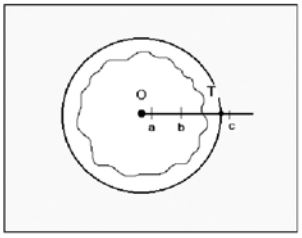

Figure 12. A schematic diagram depicting a radiodensitometric analysis using an image analyzer program.

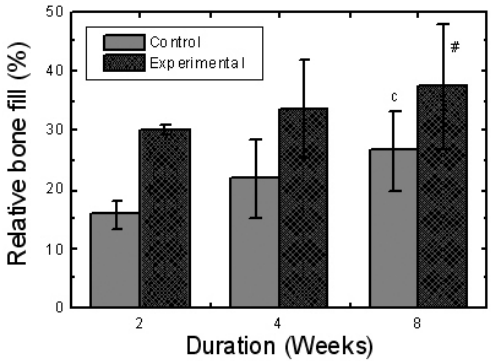

Figure 13. *Radiodensitometric analysis of the newly formed bone density.*
(#: significant difference from the control group($p<0.05$),
a: significant difference between 2 and 4 weeks($p<0.05$),
b: significant difference between 4 and 8 weeks ($p<0.05$),
c: significant difference between 2 and 8 weeks($p<0.05$)).

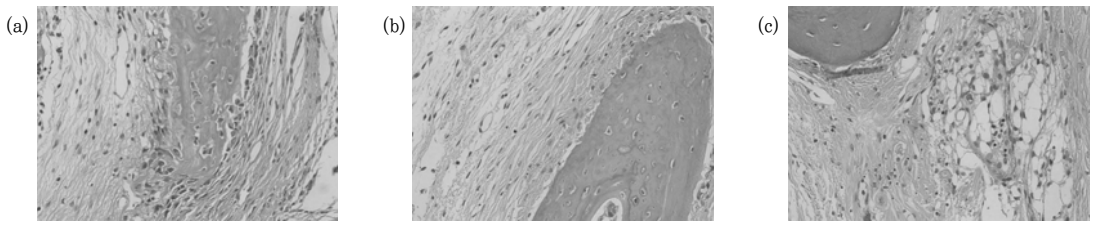

Figure 14. *Representative microphotographs of the H-E stained control group at (a) 2, (b) 4, and (c) 8 weeks postsurgery with magnification of ×200.*

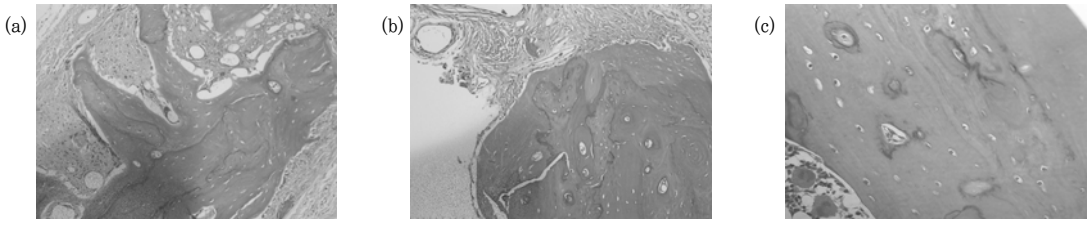

Figure 15. *Representative microphotographs of the H-E stained experimental group at (a) 2, (b) 4, and (c) 8 weeks postsurgery with magnification of ×200.*

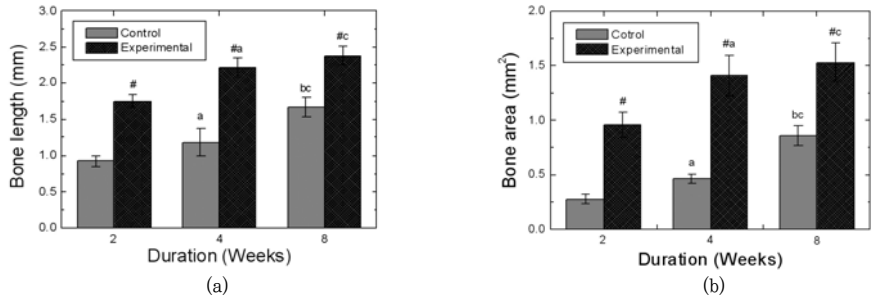

Figure. 16. *Histomorphometric analysis of (a) length and (b) area of new bone.*
(#: significant difference from the control group($p<0.05$),
a: significant difference between 2 and 4 weeks($p<0.05$),
b: significant difference between 4 and 8 weeks ($p<0.05$),
c: significant difference between 2 and 8 weeks($p<0.05$)).

Application of calcium phosphate glass to tissue engineering

1. Fabrication and structure

Calcium phosphate glass slurry was prepared by dispersing the prepared calcium phosphate glass powders into distilled water with organic additives such as binder, dispersant and a drying chemical control additive(DCCA). Polyvinyl alcohol, polyethylene glycol and dimethyl formamide were selected as binder, dispersant and drying chemical control additive, respectively[34]. First, polyvinyl alcohol (PVA; Du Pont, CA, USA) was hydrolyzed and stirred in distilled water at a temperature of 50°C at various amounts from 2 to 8wt%. After cooling to the room temperature, polyethylene glycol (PEG-400, Duksan Pure Chemical Co., Gyeonggi, Korea) was added at 5wt%, and followed by addition of dimethyl formamide (DMF; Aldrich, MO, USA) up to 10wt%. Preparation of the calcium phosphate glass slurry was completed by dispersing the glass powder into distilled water containing the organic additives from 10 to 40wt%.

Reticulated polyurethane ester sponges (Regicell, Jehil Urethane Co., Korea) were used as a template in this experiment. These sponges have 45~60 three-dimensionally interconnected open pores per linear inch. Prior to the infiltration process, the surface layer of the sponge was treated in a 2% NaOH solution for 20min ultrasonically to improve the wetting of aqueous slurry on it via improvement of hydrophilicity. With the treatment in NaOH solution, much more slurry could be homogeneously coated on the surface of sponge, due to increased surface roughness and specific surface area; this resulted in an elevated surface energy state of the sponge. There appeared to be many impurities on the surface of sponge before NaOH treatment, which may have caused non-uniformity of the slurry coating layer and given rise to defects such as abnormal grain growth during sintering. For these reasons, these impurities need to be eliminated before the slurry coating. In this current experiment, chemical treatment of sponge was best with a 2% NaOH solution for 20min, and beyond that time, the chemical degradation and spring-back properties of sponges were considerably decreased.

After cleaning and drying, the porous sponge was subjected to an infiltration process. It was immersed into the glass slurry and taken back several times, followed by rolling it through the teflon twin rollers whose spacing was controlled to compress and shrink the sponge up to 75% in thickness. This was done in order to remove the excess residual slurry from the sponge. Compressed air was blown into the pores of the sponge to perforate the clogged pores. After infiltration it was then dried at room temperature and heat-treated in a kanthal furnace. The condition of the heat-treatment was based upon a thermal analysis using TG/DTA (STA 1500, Netsch Co., Ltd., Germany). First, the temperature was raised up to 600°C very slowly at 1°C/min in order to burn out the sponge entirely, and the temperature was held there constant for 2hr to volatize the organic additives such as binder, dispersant and drying chemical control additive. Then the remaining calcium phosphate glass was sintered for 2hr at various temperatures from 650 to 850 °C. The full procedure listed above was repeated twice to thicken the framework of the porous block.

Photographs of the polymeric sponges after infiltration of the calcium phosphate glass slurry with various contents of the calcium phosphate glass powder and PVA using an optical microscope are represented in Fig. 17. When the content of the calcium phosphate glass powder was lowest as 10wt%, a thin film of the slurry clogged the pores. This was due to its low surface tension. With increasing the content of the glass powder up to 25wt%, the thin film formation was eliminated, however, the viscosity of the slurry was still low. When the content of the glass powder was fixed, coating efficacy was improved with increasing the binder content. The best condition for homogenous-thick coating of the slurry in this study

was 40wt% glass powder and 8wt% binder. This clogged pore phenomena could be also observed using a scanning electron microscope S4200, Hitachi, Japan), as is shown in Fig. 18.

PVA is used as a binder and a large amount of slurry could be coated onto the sponge as the PVA content was increased for the same powder concentration. This is because of the relatively higher powder concentration in the slurry and an increased thixotrophy are available as the PVA content is increased. For example, in case of powder concentration of 40wt% with 2wt% PVA (a relatively low binder content), the slurry coated onto sponge's surface seemed to be slightly separated into agglomerated particles and water. This is thought to happen because the added amount of binder is not enough to surround each particle effectively and also, a much higher thixotropy is required. When increasing the binder content up to 8wt%, this enabled an effective envelopment of particles and a homogeneous slurry coating behavior.

The next step for the porous scaffold fabrication is drying. Without DCCA, lots of cracks were formed and the surface of the coated film was very rough and heterogeneous, as is exhibited in Fig. 19. The surface was much smoother and more homogeneous with 5wt% DMF as the DCCA. However, the cracks were still present. When the addition of DMF increased up to 10 wt%, you can see the absolutely prevention of crack formation during the drying process.

The final step for scaffold fabrication is the heat-treatment. The role of heat-treatment is to eliminate the polymeric sponge and organic additives at a temperature of around 600°C. After that, the remaining calcium phosphate glass was sintered at various temperatures from 650 to 850°C, as is shown in Fig. 20. The glass powders sintered at 650°C just contacted with surrounding powders. With increasing the sintering temperature, the voids between the powders were decreased. You can see that the dense microstructure after sintering at 850°C is without voids and cracks.

The heating rate of as-dried porous samples turned out to be one of the important factors for obtaining successful results. The samples that were heat-treated faster than a rate of 3°C/min were collapsed locally or the samples were very weak. This resulted from a softening and elimination of the sponge before the formation of necking particles and the lack of sufficient binding strength of the particles. In case of samples heat-treated as slowly as 1°C/min, the original configuration with a three-dimensionally interconnected open pore system was maintained well after firing and the struts of porous skeletal consisted of homogeneous and dense grains.

The slurry was prepared in an aqueous system including water, and defects like cracks on the slurry coating layer may occurred on drying due to abrupt and large shrinkage caused from the high surface tension of water. In a process using a polyurethane sponge for porous ceramics, it is known that these microcracks on the coating layer may appear from a non-uniform coating thickness, the presence of a locally un-coated layer, the difference in coefficient of thermal expansion between polymeric sponge and the coated layer, the vapor pressure generated by sponge evaporation on firing or the residual internal stress due to the drying[35-36].

These are the reasons microcracks need to be controlled; otherwise, the mechanical strength will be considerably decrease due to them[37-38]. In order to control these cracks, various organic additives can be added as a DCCA. Of these additives, DMF is a very good candidate because of its lower surface tension and higher evaporation temperature when compared to those of water. Therefore, though the water evaporates on drying, DMF can be still remained between the particles and moderate local surface tension of the coating layer to prevent abrupt shrinkage, and so the microcracks can be eliminated. It was shown that microcracks did not appear with 10wt% of DMF.

As-dried calcium phosphate porous glass specimens are crystallized and sintered by heat-treatment. The

determined glass transition temperature of the glass powder was 595°C for setting up at an optimum heat-treatment temperature. The prepared porous samples were heat-treated at different temperatures ranging from 650 to 850°C. The specimen fired at 650°C showed gray color, which means that there are some remains of the sponge or additives. In contrast, sintering at 850°C enabled the specimens to be white porous glass with a dense microstructure of struts; this was thought to be the optimum firing temperature.

We repeated this process to thicken the frames of the scaffold. After sintering at 850°C, slurry was infiltrated again and dried and sintered at 850°C. With this repeating process, pore size, porosity and the thickness of struts of the scaffolds were examined by X-ray micro-computed tomography (Skyscan 1076). The scaffolds were placed with the height and width parallel to the scanning plane. The resolution was set at 35μm and an averaging of three was employed together with a filter of 0.025mm titanium, a rotation step of 0.6°, and a rotation angle of 180°. A cubical region of interest (ROI) with 3.52mm as the length and the width, and a height (approximate 3.5mm) was chosen by selecting 100 slices of scanned data for the scaffolds. After estimating the volume of the scaffold within the ROI, the empty space was obtained by subtracting the scaffold volume within the ROI from the volume of the ROI. Dividing the volume of the empty space by the volume of the ROI gave porosity[39].

Fig. 21 shows the 3D model and cross-sectional image of the 15th slice of scanned calcium phosphate glass scaffolds after once and twice processes using a polymer with 45 ppi. Fig. 22 shows the 3D model and cross-sectional image of the 15th slice of scanned calcium phosphate glass scaffolds after once and twice processes using a polymer with 60 ppi. The porosity of the calcium phosphate glass scaffolds after once and twice processes using a polymer with 45 ppi was (90.3±1.2)% and (80.7±2.3)%, respectively. The each that of the calcium phosphate glass scaffolds after once and twice processes using a polymer with 60ppi was (85.3±1.5)% and (78.7±1.0)%. The mean strut spacing, which means the pore size of the scaffold, was (703.2±17.1)μm in the calcium phosphate glass scaffold after one process using a polymer with 45ppi, (569.6±4.4)μm in the calcium phosphate glass scaffold after twice processes using a polymer with 45ppi, (390.6±11.2)μm in the calcium phosphate glass scaffold after one process using a polymer with 60ppi, and (371.6±12.8)μm in the calcium phosphate glass scaffold after twice processes using a polymer with 60 ppi. The mean strut thickness was (186.0±4.3)μm, (204.2±12.9)μm, (163.5±5.8)μm, and (171.7±2.0)μm in the calcium phosphate glass scaffolds after once and twice processes using a polymer with 45ppi and 60 ppi, respectively.

The maximum compressive load of each of the 10 porous blocks (5mm in diameter and 8mm in height) was determined by a universal testing machine (4501, Instron, USA) at 1.0mm/min of the crosshead speed. Rubber plates of 0.2mm in thickness were placed between each surface of the block and the compression punches in order to eliminate any unexpected effects due to an uneven horizontal surface level. The compressive strength was calculated from the determined maximum compressive load. As a result, the compressive strength was increased by almost two twice, as is shown in Fig. 23. However, there was no significant difference ($p>0.05$).

In summarize, macroporous calcium phosphate glass scaffold could be fabricated with 250~700mm and three-dimensionally interconnected open pore system using a polymeric sponge as a template in order to apply to the tissue engineering.

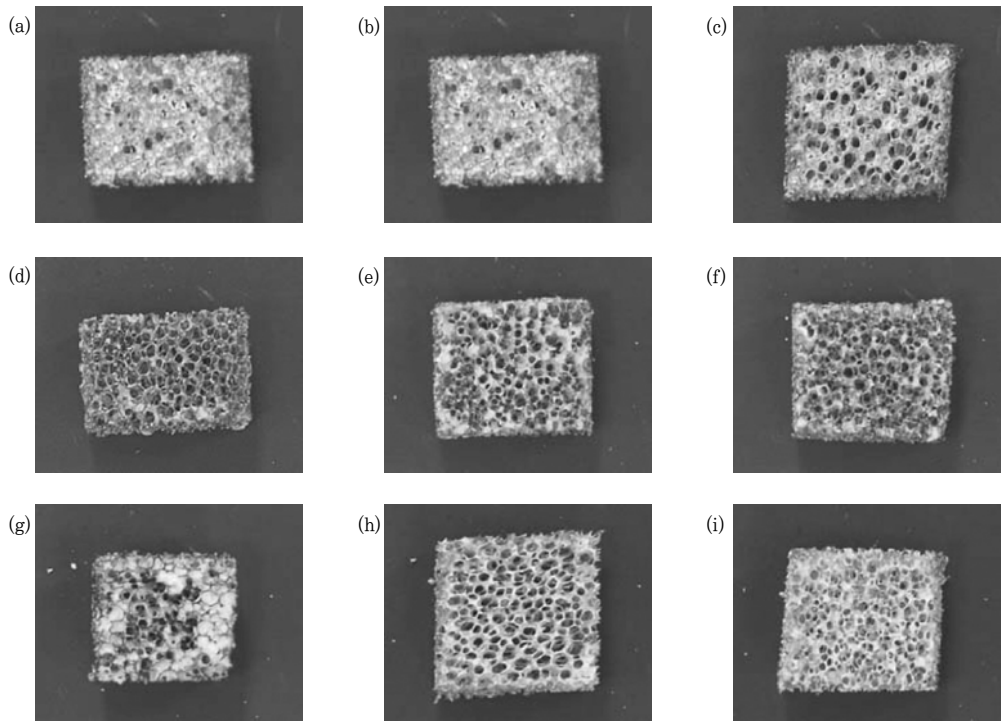

Figure 17. *Photographs of polyurethane ester sponge foams infiltrated by the calcium phosphate glass slurry with various contents of the calcium phosphate glass powder and PVA.*
(a; powder 10wt%, PVA 2 wt%, b; powder 10wt%, PVA 4wt%, c; powder 10wt%, PVA 8wt%, d; powder 33wt%, PVA 2 wt%, e; powder 33wt%, PVA 4wt%, f; powder 33wt%, PVA 8wt%, g; powder 67wt%, PVA 2 wt%, h; powder 67wt%, PVA 4wt%, i; powder 67wt%, PVA 8wt%)

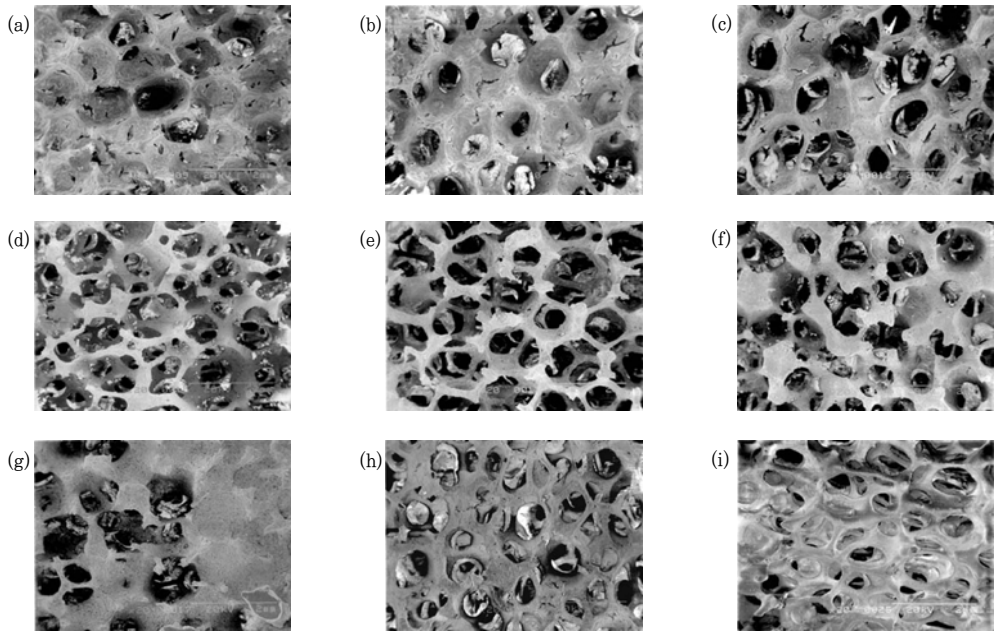

Figure 18. *SEM photographs of polyurethane ester sponge foams infiltrated by the calcium phosphate glass slurry with various contents of the calcium phosphate glass powder and PVA.*
(a; powder 10 wt%, PVA 2 wt%, b; powder 10 wt%, PVA 4 wt%, c; powder 10 wt%, PVA 8 wt%, d; powder 33 wt%, PVA 2 wt%, e; powder 33 wt%, PVA 4 wt%, f; powder 33 wt%, PVA 8 wt%, g; powder 67 wt%, PVA 2 wt%, h; powder 67 wt%, PVA 4 wt%, i; powder 67 wt%, PVA 8 wt%)

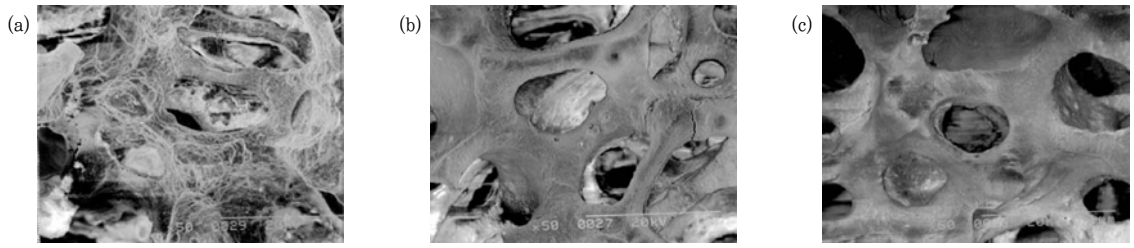

Figure 19. SEM photographs show the polyurethane ester sponge foams after infiltration and subsequent drying at 60°C with various content of dimethyl formamide. (a; 0wt%, b; 5wt%, c; 10wt%)

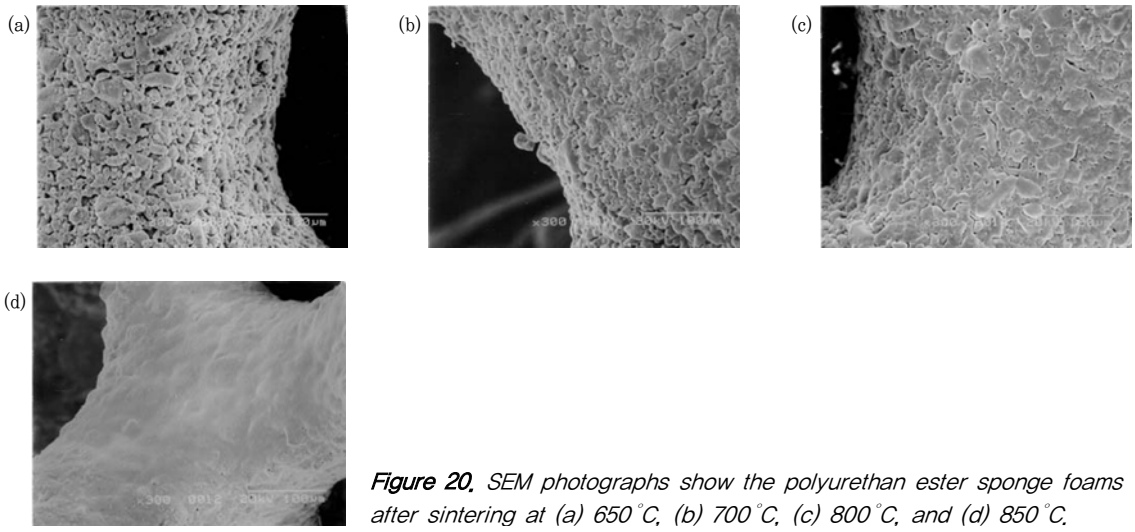

Figure 20. SEM photographs show the polyurethan ester sponge foams after sintering at (a) 650°C, (b) 700°C, (c) 800°C, and (d) 850°C.

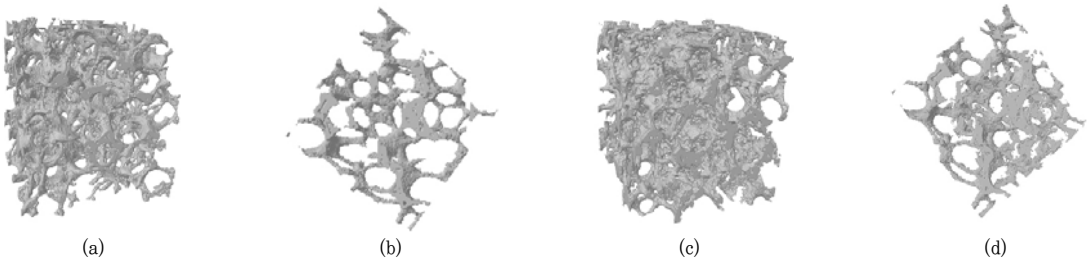

Figure 21. Images of (a, c) 3D reconstruction and (b, d) cross-section of 15th slice of the calcium phosphate glass scaffold after (a, b) once and (c, d) twice using 45 ppi sponge.

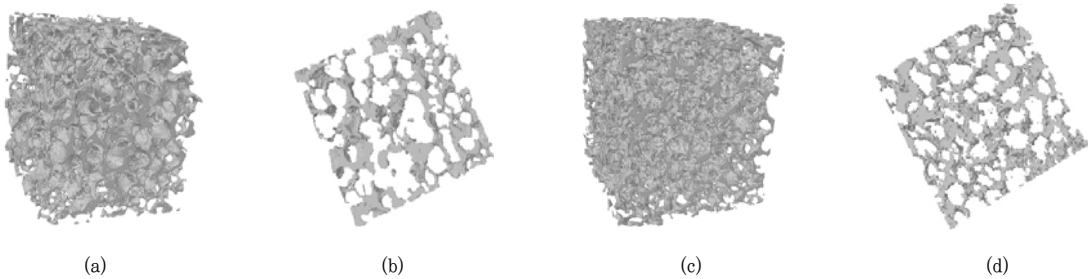

Figure 22. Images of (a, c) 3D reconstruction and (b,d) cross-section of 15th slice of the calcium phosphate glass scaffold after (a, b) once and (c, d) twice using 60 ppi sponge.

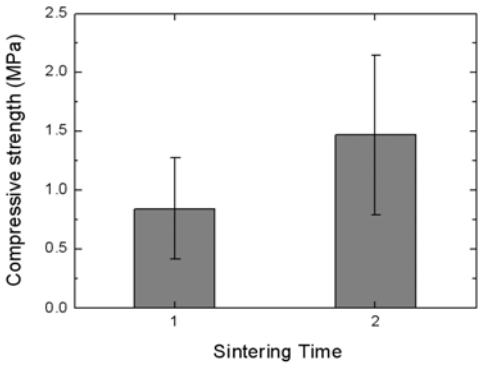

Figure 23. *Compressive strength of calcium phosphate glass scaffold after sintering at 850°C.*

2. *In vitro* test

In order to evaluate the cell affinity of the calcium phosphate glass scaffold *in vitro*, human mesenchymal stem cells(hMSCs) was cultured within the calcium phosphate glass scaffolds. Commercial HA scaffold was employed as a control in this experiment[40]. Typical SEM photographs of the calcium phosphate glass scaffold and HA scaffold are represented in Fig. 24(a) and (b), respectively.

Bone marrow cells were collected from the healthy human donors aged 4~0 years at Yonsei University Medical Center. Then the mononuclear cells were isolated by centrifugation over a Percoll density gradient (Sigma, MO, USA) at 1300rpm for 30min at 4°C. The cells were maintained in low-glucose DMEM supplemented with 10% fetal bovine serum, 100 U/ml penicillin, and 100μg/ml streptomycin in a humidified 5% CO_2 balanced-air incubator at 37°C, the media being changed every other day. On 3rd day, nonadherent marrow cells were removed by washing with phosphate-buffered saline.

Before seeding of hMSCs on the scaffolds, the scaffolds were prewetted with 70% alcohol overnight. Suspension of hMSCs was loaded on the scaffold at 1×10^6 cells/scaffold and placed on 60mm Petri dishes for 2hr. Then incubated on orbital shaker at 30rpm in a humidified 5% CO_2 balanced-air incubator at 37°C, the media being changed every other day. After 2, 4, 6, and 8 weeks, hMSCs/scaffold were fixed in 10% buffer formalin and embedded in paraffin. Each four specimens were sliced mesiodistally from paraffin blocks and stained with hematoxylin and eosin. Both extracellular matrix and the proliferative cells on the scaffolds were observed under optical microscope histologically.

The histological observations of the control and experimental groups are shown in Fig. 25~28. It was observed that the stem cells were seeded continuously proliferated both in the experimental and control groups at every incubation period. The cell counts on the 3rd and 7th day showed an increase more than twice during 4 days. The number of cells was higher in the experimental group than that of the control group at every incubation period, however, there was no significant difference ($p>0.05$). After the cells were treated with osteogenic supplements, there was a distinct decrease in the number of cells, which is analogous to the number of cells when they were incubated firstly.

On the 2nd week, definite presence of osteocalcin was found in parts of cellular cytoplasm on the 2nd week. By the 4th week, ostecalcin was detected in most of the cell's cytoplasm and diminutive amount was also found in the extracellular matrix. Following the 6th week, the intensity of ostecalcin expression within the extracellular matrix had increased. Extracellular matrices could be observed at the 2nd and 4th days in the experimental and control groups, respectively. The extracellular matrices were more abundant in the experimental group at all periods.

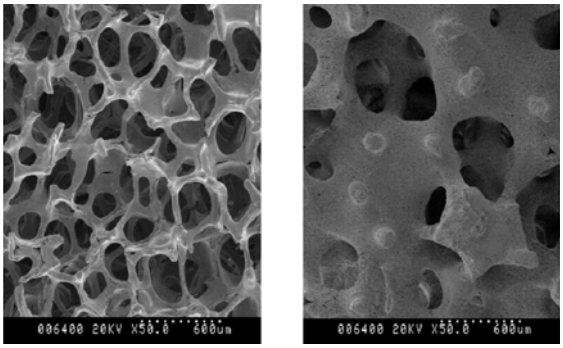

(a) (b)

Figure 24. *SEM photographs of (a) calcium phosphate glass and (b) HA scaffolds.*

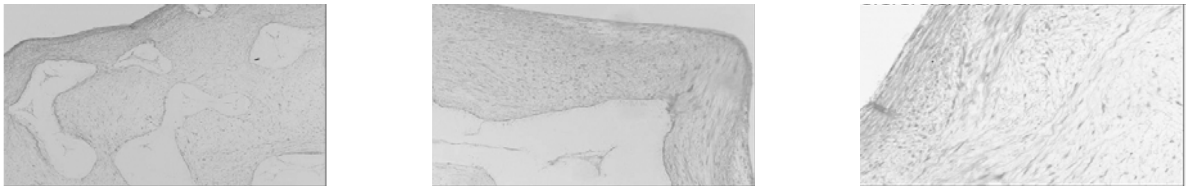

(a) (b) (c)

Figure 25. *Surgical sections of the control group after 6 weeks (a; ×4, b; ×10, c; ×20).*

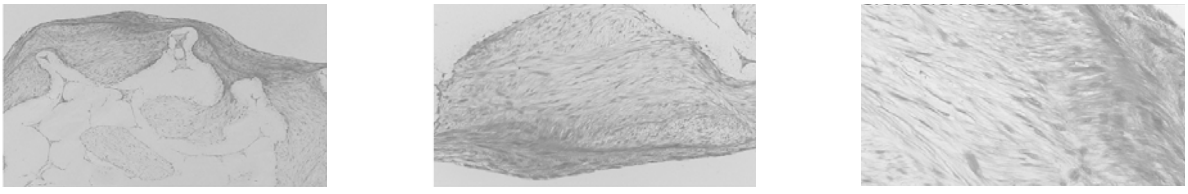

(a) (b) (c)

Figure 26. *Surgical sections of the control group after 8 weeks (a; ×4, b; ×10, c; ×20).*

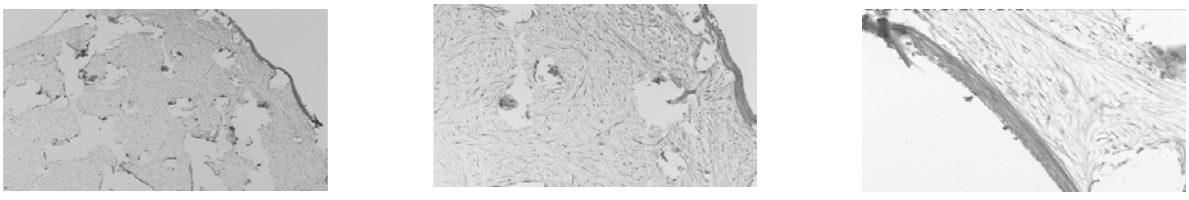

(a) (b) (c)

Figure 27. *Surgical sections of the experimental group after 6 weeks (a; ×4, b; ×10, c; ×20).*

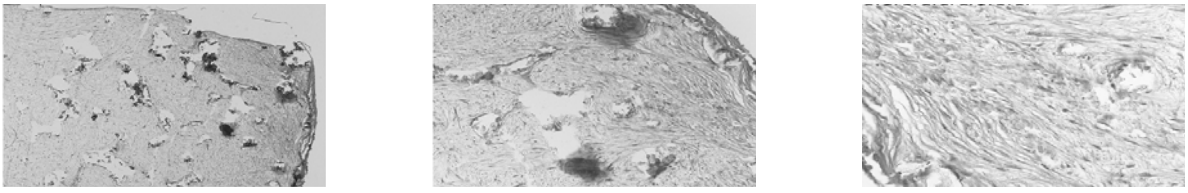

(a) (b) (c)

Figure 28. *Surgical sections of the experimental group after 6 weeks (a; ×4, b; ×10, c; ×20).*

3. *In vivo* test

Six male adult beagle dogs were used *in vivo* test of the calcium phosphate glass scaffold[41]. The surgical procedure was performed under the general anesthesia induced by the intravenous injection of atrophin (0.04mg/kg) and the intramuscular induction with the compound of xylazin and ketamin, followed by the application of enflurane through inhaling. Routine dental infiltration anesthesia (2% lidocaine hydrochloride with 1/80000 epinephrine) was used at the surgical sites. The mandibular first and third premolars had been extracted in advance of the experimental surgeries, and the extraction sites had been allowed to heal for 8 weeks. 12 intrabony defects from 6 beagle dogs with 4×4 mm 1-wall intrabony defects were surgically created in the bilateral mandibular second and fourth premolars. Following root planing, a reference notch was made with $\frac{1}{4}$ round bur on the root surface at the base of the defect. The experimental group was treated with the calcium phosphate glass scaffold and chitosan membrane together as shown in Fig. 29, while the control group was treated with a chitosan membrance without calcium phosphate glass scaffold. The subjects were sacrificed 12 weeks after surgery.

For the histometric analysis, the cementoenamel junction(CEJ) and the notch were used as reference points(bN) and the histometric parameters included defect height(DH), junctional epithelium(JE), connective tissue adhesion(CT), cementum regeneration(NC) and alveolar bone regeneration(NB) were determined as shown in Fig. 30. Histomorphometric recordings from the four sections from each defect were used to calculate mean score for each animal. Statistical analysis was compared by Mann-Whitney U test. Root resorption and ankylosis was dischotomously scored when can be observed in one or more of the four sections for each tooth.

Histologically, the juctional epithelium migrated apically, and imflammatory cell infiltration was minimal in all defect sites. Connective tissue adhesion was observed parallel to the long axis of tooth beneath the juctional epithelium. The periodontal ligament was organized mainly with irregular collagen fibers. No root resorption of ankylosis was observed in all groups as shown in Fig. 31~32. The experiemental group showed that a large amount of new cementum and new bone was formed more than that in the control group. The residual membrane was not observed in experimental group. In the experimental group, several calcium phosphate glass scaffolds remnants could be observed in the defect area and were surrounded with a provisional connective tissue which will eventually transform into bone tissue. The edge of the particles exhibited irregular features and the presence of multinucleated giant cells indicating that resorption of dissolution process. In mature new bone portion, osteoclasts observed on the surface of a secondary osteon within the bone trabeculae suggesting an active remodeling process as shown in Fig. 32(c).

The results of the histomorphometric analysis were summarized in Table 1. The amount of junctional epithelium migration was (44.51±14.46)% and (33.23 ±13.20)% in the control group and experimental group, respectively. No significant difference was found between the control group and experimental group ($p>0.05$). The amount of connective tissue adhesion was (28.57±13.91)% and (11.42±5.08)% in the control group and experimental group, respectively. No significant difference was found between the control group and experimental group ($p>0.05$). The amount of new cementum regeneration was (26.91± 13.90)% and (55.34±14.31)% in the control group and experimental group, respectively. A significant difference was observed between the control group and the experimental group ($p<0.05$). The amount of alveolar bone regeneration was (30.37±4.13)% and (52.32± 14.34)% in the control group and experimental group, respectively. A significant difference was observed between the control group and the experimental group ($p<0.05$).

The experimental group demonstrated that the significant greater gain in the bone regeneration as well as the cementum regeneration. The calcium phosphate glass scaffold resorbed and was subsequently replaced to bone tissue. This process is dynamic reconstructive healing process for bone transplantation, as it is called "creeping substitution"[42]. The resorption of the calcium phosphate glass may be the result of cell mediated phagocytosis of biologic chemical dissolution, or both[43]. Nery *et al*. reported the combination of Ca/P in the ceramic implant enhanced repopulation of cells, new periodontal tissue attachment, and bone regeneration within the space of a periodontal osseous defect[44]. It has been hypothesized that the biphasic nature of this ceramic provides two basic functions; i) initiates cell growth and differentiation, and ii) acts as a scaffold for cell maturation and bone formation; i.e., having the property of osteoinductivity[45].

In summarize, the calcium phosphate glass scaffold demonstrated the beneficial effects to 1-wall intrabony defects of beagle dogs. Based on the histological results, the calcium phosphate glass scaffold successfully functioned as an osteoconductive scaffold for invading cells of host.

Table 1. Histomorphometric Analysis of the Calcium Phosphate Glass Scaffold

	Control group		Experiment group	
	Mean	S.D.	Mean	S.D.
DH (mm)	4.41	0.42	4.92	0.62
JE/DH (%)	58.56	13.07	33.23	13.20
CT/DH (%)	10.73	5.10	11.42	5.08
NC/DH (%)	30.70	14.57	55.34*	14.31
NB/DH (%)	28.29	14.82	52.32*	14.34

*: Statistically significant difference compared with surgical control group, $P<0.05$.

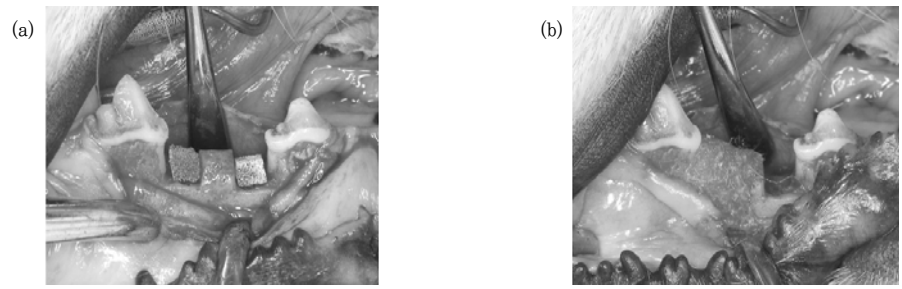

Figure 29. *Surgically created 1-wall defects treated (a) with the calcium phosphate glass scaffold and (b) subsequent covering with chitosan membrane.*

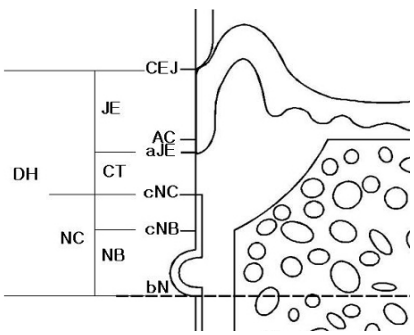

Figure 30. *A diagram depicting parameters used in histomorphometric analysis.*

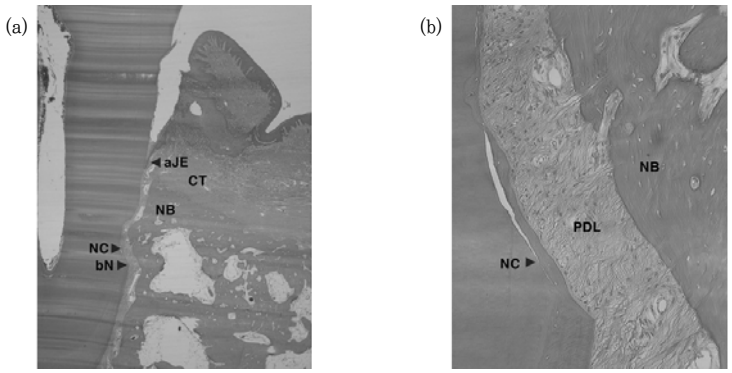

Figure 31. Surgical sections of the control group with magnification of (a) ×20 and (b) ×200.

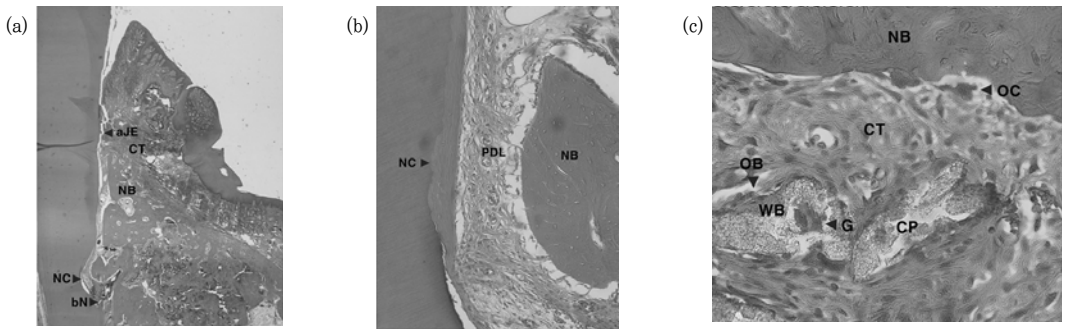

Figure 32. Surgical sections of the experimental group with magnification of (a) ×20, (b) ×200 and (c) ×400.

References

1. Brow RK. Review: the structure of simple phosphate glasses. J Non-Cryst Solids 2000;263&264:1-28.
2. Gao H, Tan T, Wang D. Effect of composition on the release kinetics of phosphate controlled release glasses in aqueous medium. J Control Release 2004;96:21-28.
3. Franks K, Abrahams I, Knowles JC. Development of soluble glasses for biomedical use. Part I: In vitro solubility measurement. J Mater Sci-Mater Med 2000;11:609-614.
4. Dias AG, Lopes MA, Gibson IR, Santos JD. In vitro degradation studies of calcium phosphate glass ceramics prepared by controlled crystallization. J Non-Cryst Solids 2003;330:81-89.
5. Hosono H, Abe Y. Porous glass-ceramics composed of a titanium phosphate crystal skeleton: a review. J Non-Crystal Solids 1995;190:185-197.
6. Knowles JC, Franks K, Abrahams I. Investigation of the solubility and ion release in the glass system K_2O-Na_2O-CaO-P_2O_5. Biomaterials 2001;22:3091-3096.
7. LeGeros RZ, Lee YK. Synthesis of amorphous calcium phosphates for hard tissue repair using conventional melting technique. J Mater Sci 2004;39:5577-5579.
8. Dayanand C, Bhikshamaiah G, Tyagaraju VJ, Salagram M, Murthy ASR. Structural investigations of phosphate glasses: a detailed infared study of the x(PbO)-(1-x)P_2O_5 vitreous system. J Mater Sci 1996;31:1945-1967.
9. Hedgens JJ, Martin SW. Glass transition and infrared spectra of low-alkali, anhydrous lithium phosphate glasses. J Am Ceram Soc 1993;76:1691-1696.
10. Khafagy AH, Ewaida MA, Higazy AA et al. Infrared spectra and composition dependence investigations of the vitreous V_2O_5/P_2O_5 system. J Mater Sci 1992;27:1435-1439.
11. LeGeros RZ. Biodegradation and bioresorption of calcium phosphate ceramics. Clin Mater 1993;14:65-88.
12. Lee YK, Song J, Lee SB *et al*. Proliferation, differentiation and calcification of preosteoblast-like MC3T3-E1 cells cultured onto non-crystalline calcium phosphate glass. J Biomed Mater Res 2004;69A:188-195.
13. Sudo H, Kodama H, Amagi Y, Yamamoto S, Kasai S. In vitro differentiation and calcification in a new clonal osteo-

genic cell line derived from newborn mouse calvaria. J Cell Biol 1983;96:191-198.
14. Quarles LD, Yohay DA, Lever LW, Caton R, Wenstrup RJ. Distinct proliferative and differentiated stages of murine MC3T3-E1 cells in culture: An in vitro model of osteoblast development. J Bone Mineral Res 1992;7:683-692.
15. Hunter A, Archer CW, Walker PS, Blunn GW. Attachment and proliferation of osteoblasts and fibroblasts on biomaterials for orthopedic use. Biomaterials 1995;16:287-295.
16. Owen TA, Aronow M, Shalhoub V *et al*. Progressive development of the rat osteoblast phenotype in vitro: Reciprocal relationship in expression of genes associated with osteoblast proliferation and differentiation during formation of bone extracellular matrix. J Cell Physiol 1990;143:420-430.
17. Lowry OH, Roberts NR, Wu ML, Hixon WS, Crawford EJ. The quantitative histochemistry of brain. J Biol Chem 1954;207:19-37.
18. Towbin H, Staehelin T, Gordon J. Electrophoretic transfer of proteins from polyacrylamide gels to nitrocellulose sheets: Procedures and some applications. Proc Natl Acad Sci USA 1979;9:4350-4354.
19. Gerstenfeld LC, Chipman SD, Glowaki J, Lian JB. Expression of differentiated function by mineralizing cultures of chicken osteoblasts. Dev Biol 1987;122:49-60.
20. Siffert RS. The role of ALPase in osteogenesis. J Exp Med 1951;93:415-425.
21. El-Ghannam A, Ducheyne P, Shapiro IM. Porous bioactive glass and hydroxyapatite ceramic affect bone cell function in vitro along different time lines. J Biomed Mater Res 1997;36:167-180.
22. Itakura Y, Kosugi A, Sudo H, Yamamoto S. Development of a new system for evaluating the biocompatibility of implant materials using an osteogenic cell line(MC3T3-E1). J. Biomed Mater Res 1988;22:613-622.
23. McGee-Russel SM. Histochemical methods for calcium. J Histochem Cytochem 1958;6:22-42.
24. Nakamura T, Yamanuro T, Higash S, Kokubo T, Itoo S. A new glass-ceramic for bone replacement: Evaluation of its bonding to bone tissue. J Biomed Mater Res 1985;19:685-698.
25. de Bruijin JD, Klein CPAT, de Groot K, van Blitterswijk CA. The ultrastructure of the bone-hydroxyapatite interface in vitro. J Biomed Mater Res 1992;26:1365-1382.
26. Moon HJ, Kim KN, Kim KM *et al*. Bone formation in calvarial defects of Sprague-Dawley rats by transplantation of calcium phosphate glass. J Biomed Mater Res 2005;74A: 497-502.
27. Freeman E, Turnbull RS. The role of osseous coagulum as a graft material. J Perio Res 1973;8:229-235.
28. Tagaki K, Urist MR. The reaction of dura to bone morphogenic protein(BMP) in repair of skull defects. Ann Surg 1982:196;100-102.
29. Schmitz JP, Hollinger JO. The critical size defect as an experimental model for craniomandibulofacial nonunions. Clin Orthop Rel Res 1986:205;299-308.
30. Marden LJ, Hollinger JO, Chauhari A *et al*. Recombinant human bone morphogenetic protein-2 is superior to demineralized bond matrix in reparting craniotomy defects in rats. J Biomed Mater Res 1994:28;1127-1138.
31. Bosch C, Melsen B, Vargervik K. Importance of the critical-sized bone defect in testing bone-regenerating materials. J Craniofac Surg 1998:9;310-316.
32. Schmitz JP, Schwartz Z, Hollinger JO, Boyan BD. Characterization of rat calvarial non-union defects. Acta Anat 1990:138;185-192.
33. Kamakura S, Sasano Y, Homma H *et al*. Implantation of octacalcium phosphate(OCP) in rat skull defects enhances bone repair. J Dent Res 1999:78;1682-1687.
34. Park YS, Kim KN, Kim KM *et al*. Feasibility of three-dimensional macroporous scaffold using calcium phosphate glass and polymeric sponge. J Mater Sci 2006:41:4357-4364.
35. Brown DD, Green DJ. Investigation of strut crack formation in open cell alumina ceramics. J Am Ceram Soc 1994:77:1467-1472.
36. Lange FF, Miller KT. Open-cell, low-density ceramics fabricate from reticulated polymer substrates. Adv Ceram Mater 1987:2:827-831.
37. Brenzy R, Green DJ. Factors controlling the fracture resistance of brittle cellular materials. J Am Ceram Soc 1991:74: 1061-1065.
38. Brenzy R, Green DJ. Fracture behavior of open-cell ceramics. J Am Ceram Soc 1989:72:1145-1152.
39. Kim MC, Kim KN, Kim KM *et al*. Application of X-ray micro-computed tomography on macroporous calcium phosphate glass scaffolds. Key Eng Mater 2006:309-311:1087-1090.
40. Kim J, Ryu JK, Kim MC *et al*. In vitro mesenchymal stem cell culture using calcium phosphate glass scaffold. Key Eng Mater 2005:284-286:679-682.

41. Min DH, Kim MJ, Yoon JH *et al*. Effect of calcium phosphate glass scaffold with chitosan membrane on the healing of alveolar bone in 1-wall intrabony defect in beagle dogs. Key Eng Mater 2005:284-286:851-854.
42. Ray RD. Bone grafts and bone implants. Otolaryngol Clin North Am 1972:5:389-398.
43. Daculsi G, LeGeros RZ, Nery E, Lynch K, Kerebel B. Transformation of biphasic calcium phosphate ceramics in vivo: ultrastructural and physicochemical characterization. J Biomed Mater Res 1989:23:883-894.
44. Nery EB, Eslami A, Van Swol RL. Biphasic calcium phosphate ceramic combined with fabrillar collagen with and without citric acid conditioning in the treatment of periodontal osseous defects. J Periodont 1990:61:166-172.
45. Nery EB, Eslami A, Van Swol RL. Biphasic calcium phosphate ceramic combined with fabrillar collagen with and without citric acid conditioning in the treatment of periodontal osseous defects. J Periodont 1992:63:729-735.